Layered Na-Ion Cathodes with Outstanding Performance Resulting from the Synergetic Effect of Mixed P- and O-Type Phases

Marlou Keller, Daniel Buchholz, and Stefano Passerini**

Herein, the synthesis of new quaternary layered Na-based oxides of the type $Na_xMn_yNi_zFe_{0.1}Mg_{0.1}O_2$ ($0.67 \leq x \leq 1.0$; $0.5 \leq y \leq 0.7$; $0.1 \leq z \leq 0.3$) is described. The synthesis can be tuned to obtain P2- and O3-type as well as mixed P-/O-type phases as demonstrated by structural, morphological, and electrochemical properties characterization. Although all materials show good electrochemical performance, the simultaneous presence of the P- and O-type phases is found to have a synergetic effect resulting in outstanding performance of the mixed phase material as a sodium-ion cathode. The mixed P3/P2/O3-type material, having an average elemental composition of $Na_{0.76}Mn_{0.5}Ni_{0.3}Fe_{0.1}Mg_{0.1}O_2$, overcomes the specific drawbacks associated with the P2- and O3-type materials, allowing the outstanding electrochemical performance. In detail, the mixed phase material is able to deliver specific discharge capacities of up to 155 mAh g^{-1} (18 mA g^{-1}) in the potential range of 2.0–4.3 V. In the narrower potential range of 2.5–4.3 V the material exhibits high average discharge potential (3.4 V versus Na/Na^+), exceptional average coulombic efficiencies (>99.9%), and extraordinary capacity retention (90.2% after 601 cycles). The unexplored class of P-/O-type mixed phases introduces new perspectives for the development of layered positive electrode materials and powerful Na-ion batteries.

1. Introduction

Nowadays, issues like climate change and depletion of fossil fuels have changed our view on the present energy production, which is essentially based on primarily nonrenewable energy sources. To ensure a stable energy supply in a worthwhile future, it will be inevitable to generate electricity to a great extent from renewable energy sources like solar and wind.[1] However, fluctuations in electricity production, resulting from the intermittency of these sources, as well as the consumption patterns, require efficient large-scale energy storage systems to ensure the stabilization of the power grid by decoupling the production and consumption of energy. As a consequence, the power grid of the future is predicted to progressively become more decentralized. Thus, energy storage systems are needed on the large scale, such as pumped hydro, conversion to hydrogen and other liquid fuels, and small scale, for which batteries are a highly promising technology.[2] In particular sodium-ion batteries (SIBs) might be an attractive candidate for cost-efficient stationary energy storage due to the cost-advantage versus lithium-ion batteries (LIBs) originating from the use of abundant, widely distributed raw materials as well as to the easy technology transfer from LIBs (the two technologies fully share the cell design as well as the assembly process) and their good electrochemical performance, being superior to most other secondary battery technologies except for LIBs.[3] SIBs appear even more promising when considering that the most commonly used battery technology for stationary energy storage is lead acid battery, which is made of highly toxic materials (Pb and H_2SO_4) and capable of storing only about 35 Wh kg^{-1}.[4] Having identified an appreciable and increasing market demand, SIBs need to be transferred into such applications, which necessitates the development of new, cheap, environmental friendly, and powerful electrode materials.

Besides polyanionic materials such as $NaFePO_4$, layered oxide compounds are particularly promising candidates for the positive electrode due to their high specific capacities.[5] Delmas et al. introduced layered sodium oxides during the 1980s and defined a structural classification for A_xMO_2-type materials (A = Li, Na; M = transition metal),[6] which describes the transition metal layers stacking arrangement and the coordination of alkali ions in it. In accordance, the octahedral or trigonal prismatic coordination of alkali ions is denoted with O and P, respectively. The number of transition metal layers per unit cell is indicated after the letter.[6] For example, O3- and P2-type phases contain octahedral sites or trigonal prismatic sites for Na^+-cations and three or two different $(MO_2)_n$-layers per unit cell,

M. Keller, Dr. D. Buchholz, Prof. S. Passerini
Helmholtz Institute Ulm (HIU)
Helmholtzstrasse 11, 89081 Ulm, Germany
E-mail: daniel.buchholz@kit.edu;
stefano.passerini@kit.edu
M. Keller, Dr. D. Buchholz, Prof. S. Passerini
Karlsruhe Institute of Technology (KIT)
P.O. Box 3640
76021 Karlsruhe, Germany

DOI: 10.1002/aenm.201501555

respectively. With the commercialization of the LIB by Sony in 1991 sodium-based layered oxides were primarily investigated as precursors for lithium analogue compounds via ion exchange.[7] However, in the last five years, research efforts and interest rapidly increased and, nowadays, a great variety of layered sodium oxides is studied as possible cathode materials for future SIBs. Research efforts focus on abundant, low-cost, and environmental friendly elements to further underline the low-cost philosophy of SIBs. Hence, elements like iron (Fe) and manganese (Mn) are intensively investigated[8] with the target to replace the more expensive and toxic elements like cobalt (Co) and nickel (Ni). In previous work we have shown that $Na_{0.45}Ni_{0.22}Co_{0.11}Mn_{0.66}O_2$ enables high specific capacities and a good overall electrochemical performance.[9,10] In further studies we demonstrated Co, the most expensive and unhealthy component, could successfully be replaced by cheap and environmental friendly Fe, which is probably also redox active at high voltages.[11,12] As a matter of fact, the resulting $Na_{0.5}Ni_{0.23}Fe_{0.13}Mn_{0.63}O_2$ material revealed excellent characteristics in terms of high capacity and cycle life. Furthermore, the effect of Mg-doping was studied for $Na_xMg_{0.11}Mn_{0.89}O_2$[13] which exhibited smoothed potential profiles, very high coulombic efficiencies, and superior long-term cyclability. It should be noted that only a low concentration of the dopant elements, such as Mg^{2+},[14] Ti^{4+}[15] or Zn^{2+},[16] is beneficial as these are electrochemically inactive and, thus, decrease the electroactive species. However, the combination of these approaches, i.e., doping with Mg^{2+} and replacement of Co^{3+} with Fe^{3+}, has not been investigated yet.

In general, pure P2- and O3-type materials show certain intrinsic advantages and drawbacks associated with their structure. The O3-type material reveals a lower reversibility above 4.0 V[17] and a lower rate performance as Na-ions have to diffuse through face-shared interstitial tetrahedral sites.[18] P2-type materials provide a lower initial sodium reservoir and a first cycle coulombic efficiency well above 100%, leading to problems regarding full cell cycling and balancing, due to a large fraction of unoccupied Na^+ ion sites.[8] These observations led us to evaluate if the intrinsic disadvantages of each material could be overcome by mixing P- and O-type phases. In the mixtures, e.g., the O3-type material would guarantee high sodium contents, whereas the P2-type structured material would contribute with its improved rate performance and higher voltage stability. Even though early studies report the coexistence of O3- and P2-type phases in dependence of the sodium content,[19] confirmed by phase diagrams studies indicating the existence of mixed-type phases,[20] so far, nearly exclusively phase pure materials were electrochemically tested and compared with each other.[21,22] Only very recent studies investigate the effect of P2- and O3-type structure coexistence, which is achieved via the partial substitution of sodium with lithium. $Na_{0.7}Li_{0.3}Ni_{0.5}Mn_{0.5}O_{2+\delta}$ was found to have a P2/O3 intergrowth structure[23] and $Na_{0.66}Li_{0.18}Mn_{0.71}Ni_{0.21}Co_{0.08}O_{2+d}$ was synthesized as a P2+O3 composite material.[24] The intergrowth material shows discharge capacities of 130 mAh g^{-1} at 15 mA g^{-1} in a potential range of 2.0–4.05 V (versus Na/Na^+), whereas the composite material exhibits a high discharge capacity of 200 mAh g^{-1} at 0.1 C (10 mA g^{-1}) in a potential range of 1.5–4.5 V (versus Na/Na^+), which, unfortunately, might be too wide to enable sodium-ion cells with reasonable voltages.

Herein, we report on the synthesis and characterization of novel layered quaternary materials of the type $Na_xMn_yNi_zFe_{0.1}Mg_{0.1}O_2$ ($0.67 \le x \le 1.0$; $0.5 \le y \le 0.7$; $0.1 \le z \le 0.3$). The materials consist of either single P2- or O3-structured layered oxides or mixture of P3-, P2-, and O3-phases. The effect of this phase coexistence on the electrochemical performance is investigated and compared to the P2-type and O3-type reference compounds, revealing the outstanding performance of specific compositions. We believe the unexplored class of P-/O-type mixtures to be highly relevant for the development of powerful cathode materials and the formulation of future Na-ion batteries.

2. Results and Discussion

2.1. Material Design

The design and development of the different $Na_xMn_yNi_zFe_{0.1}Mg_{0.1}O_2$ materials was performed considering the oxidation states of Na^+, Mn^{4+}, Ni^{2+}, Fe^{3+}, and Mg^{2+}. The initial sodium content in P2-type Na_xMeO_2 is about $x \approx 0.67$ as reported for most of the published materials.[25] The lower sodium content necessitates a higher average charge of the transition metal layer to balance the formula unit. Contrary, the initial sodium content in the O3-type structure is, most commonly, about $x \approx 1$, which allows for a lower positive charge of the transition metal layer.

In this work, small molar contents of Fe^{3+} and Mg^{2+} (0.1 equivalents each as in $Na_xMn_yNi_zFe_{0.1}Mg_{0.1}O_2$) were chosen. Mg^{2+} is electrochemically inactive but, as dopant, it enables high coulombic efficiencies and stable long-term cycling behavior.[13,14] Literature suggests superior energy efficiencies to be achieved only with smaller Fe^{3+} contents, e.g., for $Na_{0.6}Mn_{0.66}Ni_{0.22}Fe_{0.11}O_2$.[12] Therefore, the molar content of Fe^{3+} and Mg^{2+} was not varied.

The balancing of the formula can then efficiently be achieved by varying the Mn^{4+}/Ni^{2+} ratio. This, on the other hand, also allows tuning the structural properties of the material as large Mn^{4+} contents (high charge of transition metal layer) favor the P2-type structure, whereas high Ni^{2+} contents (lower charge of transition metal layer) rather lead to the O3-type material. Thus, the effect on the materials structure was investigated by changing the Mn^{4+}/Ni^{2+} ratio, while keeping their molar sum at 0.8, in order to obtain a sodium molar content equal to 1 for the O3-type material and 0.667 for the P2-type material. Considering the well-known, although minor, formation of Mn^{3+}, a slightly higher molar amount of Mn was used in order to guarantee the appropriate charge balance and obtain phase pure P2-type and O3-type materials. Based on this consideration, the compositions $Na_{2/3}Mn_{0.7}Ni_{0.1}Fe_{0.1}Mg_{0.1}O_2$ and $Na_1Mn_{0.5}Ni_{0.3}Fe_{0.1}Mg_{0.1}O_2$ were targeted to achieve P2-type and O3-type materials, respectively.

The initial synthesis of the different materials indicated that a higher initial stoichiometric sodium content leads to O3-type structures (see Supporting Information Figure S1). Furthermore, the P2-type material was found to form when the materials were slowly cooled down in the furnace. Consequently, choosing intermediate parameters (slow cool down in the furnace instead of quenching in liquid nitrogen; stoichiometric

sodium content of 0.76 eq. of Na^+ instead of 0.67 eq. or 1.0 eq. Na^+ for P2- or O3-type material, respectively) was expected leading to a material composed of mixed P- and O-type layered oxides. Very important is that the synthesis of the material was conducted under "equilibrium chemistry" conditions as reported by Paulsen and Dahn in 1999.[7] As a matter of fact, high temperatures and reaction times long enough to ensure the formation of thermodynamically stable phases were applied. This results in the formation of P-type and O-type phases, each in its most stable elemental composition. However, the process is limited by the average elemental availability of $Na_{0.76}Mn_{0.5}Ni_{0.3}Fe_{0.1}Mg_{0.1}O_2$. Also, the different phases form via competing reactions, influencing their final ratio.

In the following, the investigations will focus on the characterization of P2-$Na_{2/3}Mn_{0.7}Ni_{0.1}Fe_{0.1}Mg_{0.1}O_2$, O3-$Na_1Mn_{0.5}Ni_{0.3}Fe_{0.1}Mg_{0.1}O_2$, and the mixed P3/P2/O3-type structured material with an average elemental composition of $Na_{0.76}Mn_{0.5}Ni_{0.3}Fe_{0.1}Mg_{0.1}O_2$.

2.2. Structural and Morphological Characterization

Initially, inductively coupled plasma optical emission spectrometry (ICP-OES) was performed to verify the elemental composition of the different as-prepared materials. **Table 1** gives an overview about the structure of the materials, their synthesis conditions, and the ICP-OES results. Results are in good accordance with the targeted stoichiometry as the variation of the elemental content, mostly, is only about ±0.01 (P2-$Na_{0.67}Mn_{0.69}Ni_{0.11}Fe_{0.09}Mg_{0.11}O_2$). However, for O3-$Na_1Mn_{0.5}Ni_{0.3}Fe_{0.1}Mg_{0.1}O_2$ and for the mixed P3/P2/O3-$Na_{0.76}Mn_{0.5}Ni_{0.3}Fe_{0.1}Mg_{0.1}O_2$ slightly lower Na contents were found ($Na_{0.83}Mn_{0.51}Ni_{0.31}Fe_{0.08}Mg_{0.10}O_2$ and $Na_{0.72}Mn_{0.51}Ni_{0.31}Fe_{0.08}Mg_{0.09}O_2$, respectively).

X-ray diffractograms (**Figure 1**) and Rietveld refinement prove the aforementioned considerations for the structural design to be reasonable. All materials could be successfully synthesized (Figure 1) with only small amounts of additional crystalline phases. The Rietveld refinements, incorporating also these phases and revealing their small content, are given in Supporting Information Figure S2.

In more detail, $Na_{2/3}Mn_{0.7}Ni_{0.1}Fe_{0.1}Mg_{0.1}O_2$ with higher Mn^{4+}/Ni^{2+} ratio has a P2-type structure (space group: $P6_3/mmc$) with calculated lattice parameters of $a = 2.885$ Å and $c = 11.209$ Å (Figure 1a). The reflections of a hexagonal impurity (O3-type structure, space group: $R\bar{3}m$) are marked with circles. The X-ray diffraction (XRD) pattern of $Na_1Mn_{0.5}Ni_{0.3}Fe_{0.1}Mg_{0.1}O_2$ confirms the O3-type structure (space group: $R\bar{3}m$) (Figure 1b). The calculated lattice parameters are $a = 2.947$ Å and $c = 16.130$ Å. The reflections of a minor cubic impurity (space group: $Fm\bar{3}m$) are marked with squares.

Most importantly, intermediate synthesis parameters, indeed, lead to a mixture of the P3-type (space group: $R3m$), P2-type (space group: $P6_3/mmc$), and O3-type (space group: $R\bar{3}m$) structures for $Na_{0.76}Mn_{0.5}Ni_{0.3}Fe_{0.1}Mg_{0.1}O_2$. Interestingly, the presence of a cubic phase (space group: $Fm\bar{3}m$; marked with a square in Figure 1c) is evidenced as well. Calculated lattice parameters via Rietveld refinement are $a = 2.8997$ Å and $c = 16.6866$ Å for the P3-type phase, $a = 2.901$ Å and $c = 11.121$ Å for the P2-type material, and $a = 2.933$ Å and $c = 16.353$ Å for the O3-type material. The P2-type layered oxide exhibits a smaller c parameter in this mix (in comparison to the pure P2-type material) due to the higher Na content and, consequently, weaker repulsion of adjacent oxygen layers. In the same manner, the c parameter is larger for the O3-type material in the mix as it contains a lower Na content compared to the pure O3-type material. The a parameter shows only slight changes when comparing the mixed and the pure materials as it is less dependent on the Na content. The relative ratio between P- and O-type phases, as obtained via Rietveld refinement, is 41% (P): 49 % (O). The cubic phase has a very similar composition as the one within the pure O3-type material and Rietveld refinement indicates its share of 10%. Energy-dispersive X-ray spectroscopy (EDX) investigations suggest the cubic phase to be MgO as small accumulations of Mg are detected (Supporting Information Figure S3). However, both NiO and MgO exhibit the cubic space group of $Fm\bar{3}m$ but differ in their lattice parameter a which is 4.177 Å for NiO[26] and 4.212 Å for MgO.[27] The lattice parameter of the cubic impurity is $a = 4.189$ Å. Hence, a mixture of both components was obtained, most likely with a composition of $Mg_{1-x}Ni_xO$ ($x \approx 0.3$) when comparing the lattice parameter with literature[27] Also, the rather broad diffraction peaks indicate a mixture of MgO and NiO as a variety of interlayer distances exists.[28] MgO coatings are known to enhance the cycling stability as they act as a barrier between the electrolyte and the active material preventing dissolution of active species.[29,30] Also the addition of $Mg_{1-x}Ni_xO$ was found to result in an improved cycle reversibility of layered oxides.[28]

Scanning electron microscopy (SEM) images for P2-$Na_{2/3}Mn_{0.7}Ni_{0.1}Fe_{0.1}Mg_{0.1}O_2$, O3-$Na_1Mn_{0.5}Ni_{0.3}Fe_{0.1}Mg_{0.1}O_2$, and the mixed P3/P2/O3-$Na_{0.76}Mn_{0.5}Ni_{0.3}Fe_{0.1}Mg_{0.1}O_2$ material are depicted in **Figure 2**. The P2-type material is composed of flake like primary particles with sharp edges of around 1–3 µm in diameter and 100–500 nm in length (Figure 2a,b). On the contrary, the O3-type material particles (Figure 2c,d) are smaller (around 0.5–1 µm) and appear more spherical and agglomerated. Furthermore, an amorphous shell covering the particle surface is visible, known to be composed of sodium carbonate.[31] Finally, and most importantly, SEM clearly confirms the mixture of P3-/P2-/O3-type layered oxides (Figure 2e,f). Besides the larger flakes of around 1–4 µm in diameter, belonging to the P2-type material, also the smaller (0.5–1 µm) particles of the O3- and P3-type material are apparent. The combination of the larger flakes and smaller spherical particles suggests a more effective utilization of the interstices inside the material.

Table 1. Overview about the materials that were synthesized, the corresponding synthesis condition, and ICP-OES results.

Structure types	Synthesis conditions	Compositions and ICP-OES results
P2	Solid state reaction (800 °C) + slow cool-down in furnace	$Na_{2/3}Mn_{0.7}Ni_{0.1}Fe_{0.1}Mg_{0.1}O_2$ $Na_{0.67}Mn_{0.69}Ni_{0.11}Fe_{0.09}Mg_{0.11}O_2$
O3	Solid state reaction (900 °C) + quenching in $N_{2(l)}$	$Na_1Mn_{0.5}Ni_{0.3}Fe_{0.1}Mg_{0.1}O_2$ $Na_{0.83}Mn_{0.51}Ni_{0.31}Fe_{0.08}Mg_{0.10}O_2$
P3/P2/O3-material	Solid state reaction (900 °C) + slow cool-down in furnace	$Na_{0.76}Mn_{0.5}Ni_{0.3}Fe_{0.1}Mg_{0.1}O_2$ $Na_{0.72}Mn_{0.51}Ni_{0.31}Fe_{0.08}Mg_{0.09}O_2$

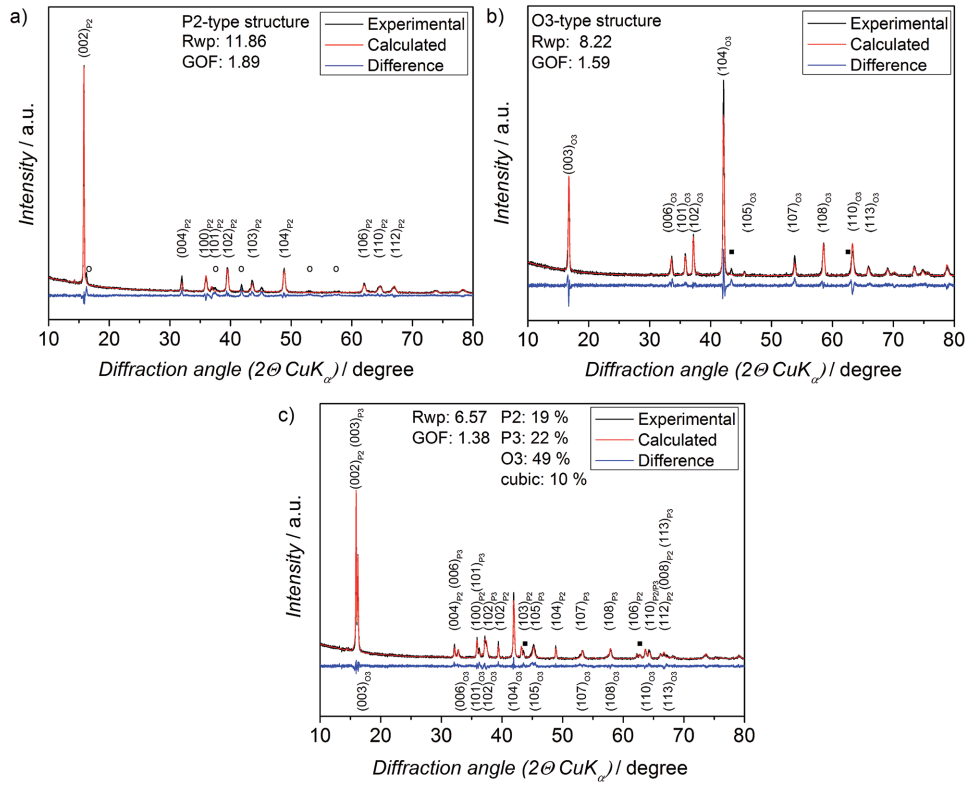

Figure 1. X-ray diffraction pattern and Rietveld refinement of a) P2-type $Na_{2/3}Mn_{0.7}Ni_{0.1}Fe_{0.1}Mg_{0.1}O_2$ (minor impurity of an O3-type phase is marked with o). b) O3-type $Na_1Mn_{0.5}Ni_{0.3}Fe_{0.1}Mg_{0.1}O_2$ (minor cubic phase is marked with squares), and c) P3/P2/O3-material (cubic $Mg_{1-x}Ni_xO$ ($x \approx 0.3$) phase is marked with squares).

2.3. Electrochemical Characterization

The electrochemical (de-)sodiation of the various as-prepared materials was initially evaluated via cyclic voltammetry (**Figure 3**). The cyclic voltammograms reveal the complex electrochemical behavior of the different materials, indicating that the transition metals are active in wide potential ranges.[32–34] This is mainly because the arrangement of the four elements (Mn, Ni, Fe, and Mg) in the transition metal layer results in a great variety of local environments.[35] This variety of environments and the electrostatic repulsion of the sodium cations, both causing sodium-vacancy ordering,[36] lead to the reversible (de-)intercalation of sodium cations to occur over a wide range of potentials.[37]

Additionally, sodium sites of different energy (i.e., taking up and releasing Na^+ cations at different potentials) exist in the P2-type structure.[37] Furthermore, the presence of different phases (P3, P2, O3) leads to a more complex electrochemical behavior. For all these reasons, broad or multiple peaks of similar intensity instead of sharp, well-separated peaks are observed. Nevertheless, broad potential ranges in which each transition metal is redox active could be assigned based on literature.[12,32,33,35,38] In the lower potential region (2.0–2.5 V) the anodic and cathodic current peaks are associated with the Mn^{3+}/Mn^{4+} redox process.[32,33,35] In the potential range of 2.5–4.3 V the double electron process of the Ni^{2+}/Ni^{4+} redox couple takes place.[12,32,38] In addition, other works on similar layered $Na_xFe_xMn_{1-x}O_2$ materials demonstrated that the current peaks at higher potentials might also be associated with the Fe^{3+}/Fe^{4+} redox couple as Fe^{4+} was detected at higher potentials (3.9–4.3 V).[32,33] However, further investigations are necessary to clarify if Fe also participates in the redox process in these materials.

Upon consecutive cyclic sweeps, most current peaks remain constant and show very good reversibility. Only some peaks show a slight decrease of the specific current accompanied by slight shifts to higher potentials or a slight broadening. A slightly lower reversibility is observed for the current peak at higher potentials (about 4.2 V) which is known to be accompanied by structural transitions[39] which will be explained in greater detail below. However, the current peak is still quite reversibly obtained for all materials. Indeed, compared to other materials, the peak at high potentials is much more reversible.[15,17,32,40]

The voltammogram of P2-$Na_{2/3}Mn_{0.7}Ni_{0.1}Fe_{0.1}Mg_{0.1}O_2$ (Figure 3a) exhibits a series of current peaks that can be paired due to a symmetric shape of the cyclic sweep (2.1 V/<2.0 V (anodic/cathodic), 2.3 V/2.2 V, 2.5 V/2.3 V, 2.8 V/2.6 V, 3.15 V/3.1 V, 3.35 V/3.3 V, 3.6 V/3.5 V, 3.9 V/3.7 V, 4.25 V/3.9 V). The intense specific current peak at 2.1 V is a result of the higher manganese content and, thus, increased participation of the Mn^{3+}/Mn^{4+} redox couple in the overall electrochemical redox process in comparison to the other two materials. However, the intensity decreases from the 2nd to the 20th cyclic

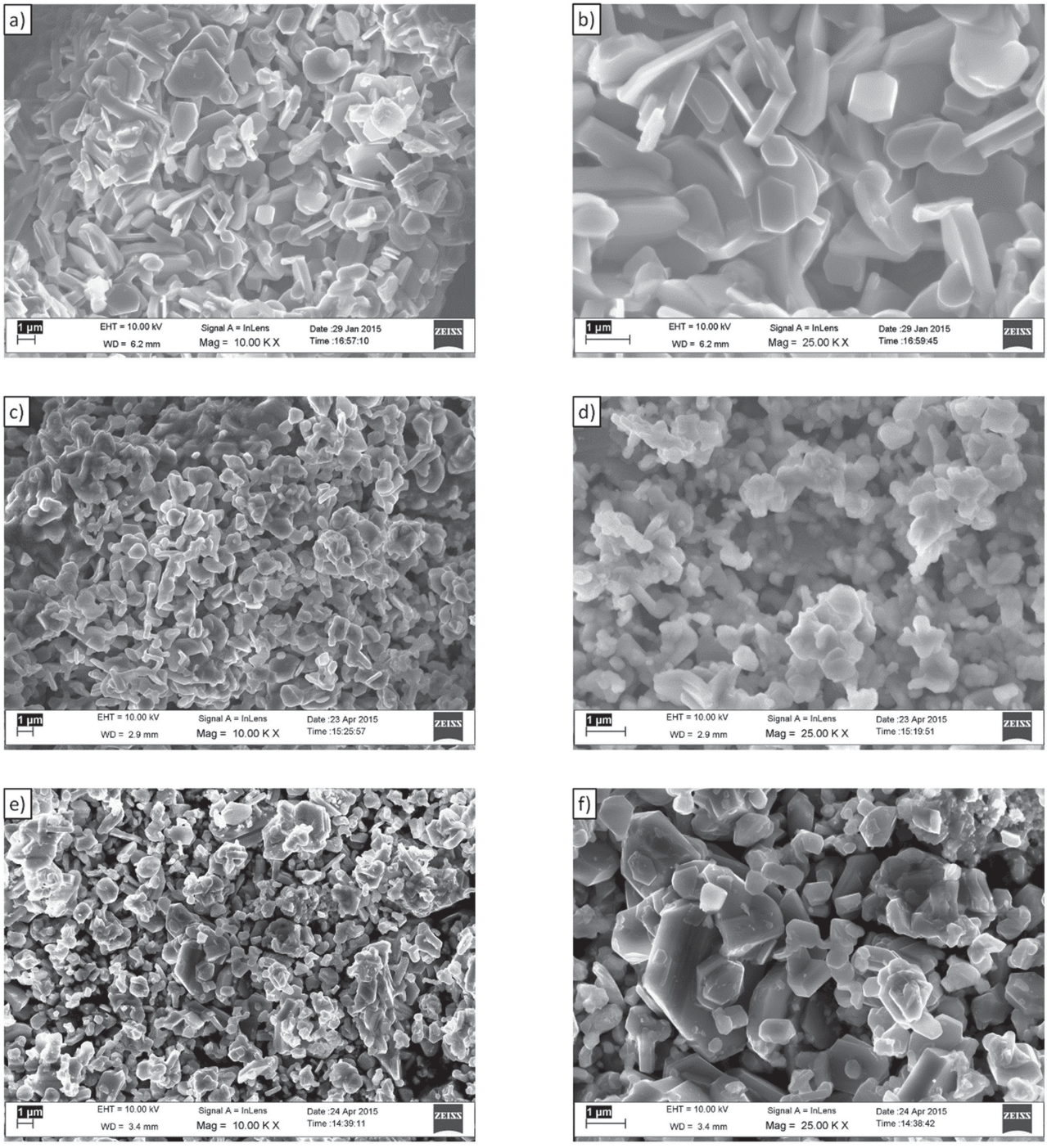

Figure 2. SEM images of a,b) P2-$Na_{2/3}Mn_{0.7}Ni_{0.1}Fe_{0.1}Mg_{0.1}O_2$, c,d) O3-$Na_1Mn_{0.5}Ni_{0.3}Fe_{0.1}Mg_{0.1}O_2$, and e,f) P3/P2/O3-material obtained at lower (left images) and higher (right images) magnification.

sweep with the anodic peak maximum shifting to higher potentials, leading to an increasing current in the potential range of 2.25–3.0 V. This suggests an increasing polarization and irreversible structural changes (e.g., Mn^{2+} dissolution due to disproportionation of Mn^{3+}). Upon consecutive cycling sweeps, the anodic peak at 4.25 V slowly decreases in intensity and slightly shifts to higher potentials suggesting the phase transition upon charging[39] to be partially irreversible.

The voltammogram of O3-$Na_1Mn_{0.5}Ni_{0.3}Fe_{0.1}Mg_{0.1}O_2$ (Figure 3b) exhibits only three features per sweep with potential maxima at 2.9 V/2.6 V, 3.5 V/3.0 V, and 4.2 V/3.8 V. In the lower potential region only a small and very symmetric current peak is revealed proving a minor but stable contribution of the Mn^{4+}/Mn^{3+} redox process. Contrary to the P2-type material, the highest peak current is observed at 2.9 V, which can be associated with the higher Ni^{2+} content. The peak at 4.25 V strongly

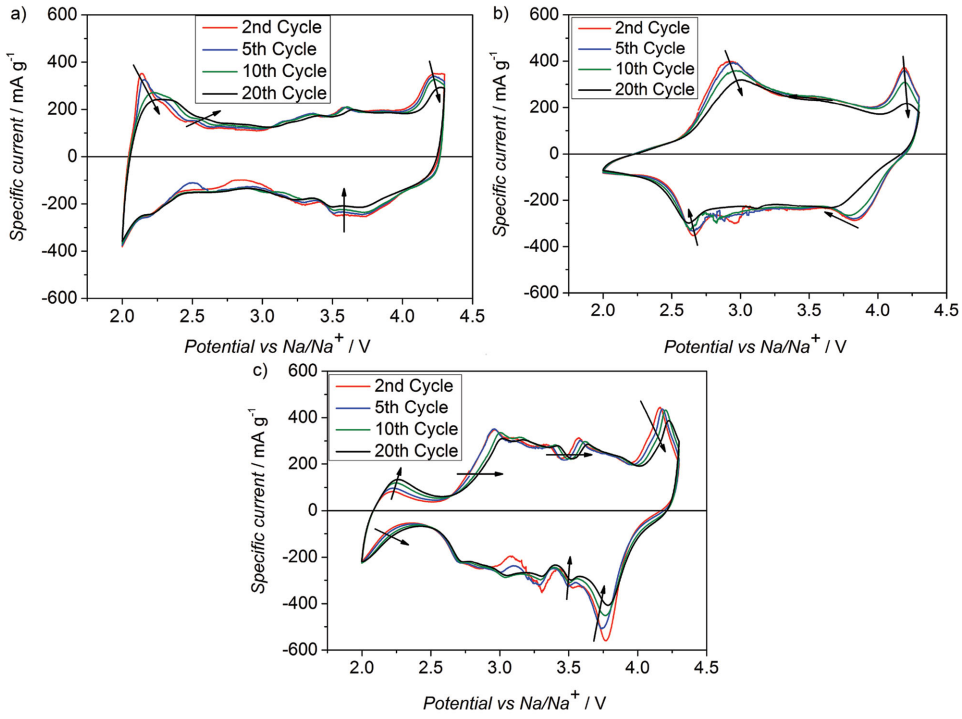

Figure 3. Cyclic voltammograms of selected cyclic sweeps of a) P2-$Na_{2/3}Mn_{0.7}Ni_{0.1}Fe_{0.1}Mg_{0.1}O_2$, b) O3-$Na_1Mn_{0.5}Ni_{0.3}Fe_{0.1}Mg_{0.1}O_2$, and c) P3/P2/O3-material. Scan rate: 1 mV s^{-1}. Potential range: 2.0–4.3 V versus Na/Na^+. Reference and counter electrode: Na. Temperature: 20 ± 2 °C. Electrolyte: 1 M $NaPF_6$ in PC. Active material mass loading: P2) 3.99 mg, O3) 3.67 mg, P3/P2/O3-material) 4.16 mg.

decreases in intensity. This is suggesting the phase transition (from P′3 to P″3 upon charging derived from the previous O3-P3 phase transition) to be more irreversible, which is in accordance with previous reports on O3-type materials cycled above a potential of 4.0 V.[17]

The voltammogram of mixed P3/P2/O3-$Na_{0.76}Mn_{0.5}Ni_{0.3}Fe_{0.1}Mg_{0.1}O_2$ (Figure 3c) reveals a series of current peaks with maxima at 2.2 V/2.0 V, 3.0 V/2.7 V, 3.1 V/2.85 V, 3.3 V/3.0 V, 3.6 V/3.3 V, 3.8 V/3.5 V, 4.1 V (peak shoulder), and 4.2 V/3.8 V. In detail, an additional peak shoulder at 4.1 V is observed for the anodic peak at 4.2 V suggesting the phase transition to be more complicated as the structural transition of all parent phases has to be taken into account. Most important, the voltammogram of the mixed P3/P2/O3-materials resembles those of P2-$Na_{2/3}Mn_{0.7}Ni_{0.1}Fe_{0.1}Mg_{0.1}O_2$ and O3-$Na_1Mn_{0.5}Ni_{0.3}Fe_{0.1}Mg_{0.1}O_2$.

Figure 4a reports the 1st cycle of galvanostatic (de-)sodiation of the various $Na_xMn_yNi_zFe_{0.1}Mg_{0.1}O_2$ ($0.67 \leq x \leq 1.0$; $0.5 \leq y \leq 0.7$; $0.1 \leq z \leq 0.3$) materials at 0.1 C (18 mA g^{-1}) in the potential range of 2.0–4.3 V. The potential profiles of all materials exhibit smooth slopes. This sloping nature of the plateau is known to result from the Mg doping.[13,14] The first specific charge capacity provides information about the initially extracted sodium content, which was calculated according to the Faraday's law excluding parasitic side reactions to occur (due to the low C rate, 0.1 C, kinetic limitations were also excluded). The

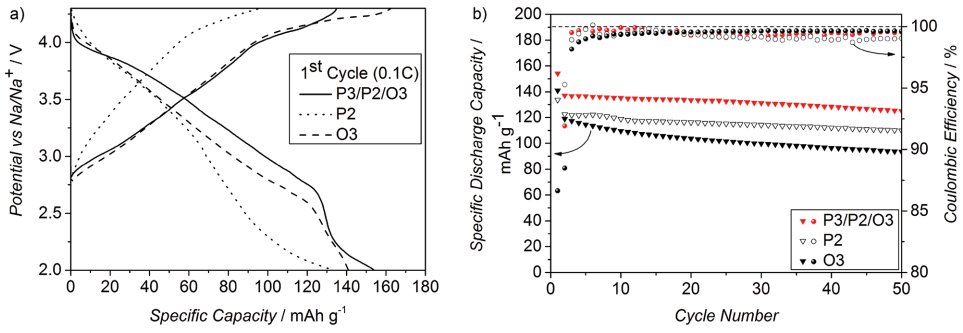

Figure 4. Galvanostatic cycling of P2-$Na_{2/3}Mn_{0.7}Ni_{0.1}Fe_{0.1}Mg_{0.1}O_2$, O3-$Na_1Mn_{0.5}Ni_{0.3}Fe_{0.1}Mg_{0.1}O_2$, and P3/P2/O3-material at 1 C (180 mA g^{-1}) except for the 1st cycle (0.1 C). a) Potential profiles of the 1st cycles, and b) specific discharge capacities and coulombic efficiencies versus cycle number for 50 cycles. Potential range: 2.0–4.3 V versus Na/Na^+. Reference and counter electrode: Na. Temperature: 20 ± 2 °C. Electrolyte: 1 M $NaPF_6$ in PC. Active material mass loading: P2) 3.99 mg, O3) 3.72 mg, P3/P2/O3-material) 4.16 mg.

highest initial charge capacity is delivered by the O3-type material (162.8 mAh g^{-1}, i.e., 0.66 eq. of Na^+) which, in fact, also contains the largest initial sodium reservoir. However, the voltage plateau at 4.1 V upon charge suggests irreversible structural changes to occur above 4.0 V as the corresponding voltage plateau is much shorter during discharge.[40] The P2-type material shows a lower first specific charge capacity (95.8 mAh g^{-1}, i.e., 0.36 eq. of Na^+) due to the lower sodium content (0.67 eq. Na^+). Interestingly, the mixed P3/P2/O3 material reveals increased structural stability with respect to the O3-type material (continuous potential increase above 4.0 V) and higher specific charge capacity (135.1 mAh g^{-1}, i.e., 0.52 eq. of Na^+) compared to the P2-type material.

Upon sodiation, the average discharge potential is higher for the O3-type and mixed P3/P2/O3 materials (both 3.2 V) and lower for the P2-type material (3.0 V) due to the increased participation of the Mn^{3+}/Mn^{4+} redox process. More detailed information can be found in Table S2 in the Supporting Information. The coulombic efficiency of the 1st cycle is only 87% for the O3-type material, in accordance with the observed irreversibility at higher potentials. On the contrary, the P2-type and mixed P3/P2/O3 materials reveal coulombic efficiencies above 100% for the 1st cycle (140% and 114%, respectively) due to the lower initial sodium reservoir in the P-type structures.

Upon galvanostatic cycling at 1 C in the potential range 2.0–4.3 V (Figure 4b) high specific discharge capacities as well as coulombic efficiencies that exceed 99% after the 10th cycle are shown by all materials. In more details, the P2-type material exhibits specific discharge capacities of 122.4 mAh g^{-1} and 110.0 mAh g^{-1} at the 2nd and 50th cycle, resulting in 89.9% capacity retention (2nd–50th cycles). These results are clearly better than those of the O3-type material, which exhibits specific discharge capacities of 118.9 mAh g^{-1} and 93.4 mAh g^{-1} for the 2nd and 50th cycles resulting in a capacity retention of only 78.6%. However, the mixed P3/P2/O3-material shows a superior capacity retention of about 91.3% and the highest discharge capacities in the 2nd and 50th cycles (137.0 mAh g^{-1} and 125.1 mAh g^{-1}, respectively). Table S3 in the Supporting Information summarizes the results for a better overview. This outstanding performance, in accordance with the observations during the first galvanostatic cycle, is indicative of a synergetic effect induced by the coexistence of the P-type and O-type phases.

The capacity fading of phase pure layered oxides upon cycling results from the occurring phase transitions, which are accompanied by large volume changes. These have a major impact, especially if these phase transitions occur at high potentials. In fact, the *c*-axis parameter of layered Na-based oxides is known to change dramatically upon sodium (de-)intercalation and phase transitions with the latter usually observed at higher potentials. In detail, the *c*-axis parameter of the O3-type material increases by ≈+1.7 Å[17] upon the several phase transitions leading to the final P″3-type material (fully charged state). In the opposite manner, the *c*-axis parameter of the P2-type material decreases (≈–2.5 Å)[39,41] as the material undergoes the phase transition to O2-type upon charge. A similar trend occurs for the P3-type material above 4.0 V.[10,42] However, the opposite volumes' changes occurring in the P-type and O-type phases (which have a ratio of 41/49 as indicated by the Rietveld refinement) result in a very moderate overall electrode volume change. This reduces the strain inside the electrode, leading to the superior reversibility and capacity retention of the mixed material. To verify this hypothesis, however, in situ XRD measurements will be performed and reported in a following manuscript. **Figure 5** reports the electrochemical behavior of the three $Na_xMn_yNi_zFe_{0.1}Mg_{0.1}O_2$ ($0.67 \leq x \leq 1.0$; $0.5 \leq y \leq 0.7$; $0.1 \leq z \leq 0.3$) materials upon C-rate tests at current rates of 0.1, 0.2, 0.5, 1, 2, 5 C and ending with 0.2 C (1 C corresponding to a specific current of 180 mA g^{-1}) within the potential range 2.0–4.3 V. The resulting specific discharge capacities (Figure 5a) obtained for the P2-, O3-, and mixed P3/P2/O3 material at different C-rates are shown in **Table 2**. Interestingly, the highest specific capacities are always delivered by the mixed P3/P2/O3-material independently from the applied current rate due to the favorable combination of the high Ni content enhancing the performance of the O3-type phase[12] and the enhanced Na-ion diffusion characteristics of the P2-type phase.

The average discharge potential for the P2-, O3-, and mixed P3/P2/O3 material is 3.0, 3.2, and 3.2 V (versus Na/Na^+) at 0.1 C (3rd cycle), respectively. This leads to theoretical specific energies of 388.3, 416.9, and 489.7 Wh kg^{-1}, respectively, considering the weight of the active material only. In line with previous results, the mixed P3/P2/O3 material shows the highest theoretical specific energy (see also Table S4 in the Supporting Information). The capacity retention after the C-rate test (comparing the 7th and 32nd cycles; both 0.2 C) is the highest for the mixed P3/P2/O3-material (99.3%). Lower values are obtained for the capacity retention of the P2- and O3- type materials (95.4% and 94.9%, respectively).

The discharge potential profiles for all materials (Figure 5b–d) reveal an ohmic drop as high as 0.4 V for the P2-, 0.5 V for the O3- and only about 0.25 V for the mixed P3/P2/O3 material at higher current rates (5 C, 27th cycle). The smallest overpotential is apparent for the mixed P3/P2/O3-material, explaining the high delivered capacities during the C-rate test. With increasing C-rate the plateau initially at 2.2 V, which are associated with the Mn^{3+}/Mn^{4+} redox process, shift below the lower cut-off potential during discharge. The effect of this shift is more pronounced for the P2-type material at high rates (5 C, 900 mAh g^{-1}) due to its higher Mn content. Similarly, the plateau above 4.0 V shifts toward and, finally, above the upper cut-off potential during charge as higher current rates were applied.

The previous investigations clearly reveal the superior performance of the mixed P3/P2/O3 material in terms of delivered specific capacity, average discharge potential, rate capability, capacity retention, and coulombic efficiencies. Interestingly, a blend of the P2-type and O3-type materials does not deliver such improved performances compared to the synthesized mixed P3/P2/O3 material (Figure S4 in Supporting Information). This confirms the importance to synthesize mixed multiphase materials under equilibrium conditions to obtain this synergetic effect. Consequently, the mixed P3/P2/O3 material was studied in greater details, in particular to address the issue of the slight but still observable capacity fading upon long-term cycling (Figure 5a). This capacity loss can mostly be attributed to the shifting of the potential plateau at 2.1 V (attributed to the Mn^{3+}/Mn^{4+} redox couple) below the lower cut-off potential upon discharge. The corresponding potential profiles can be

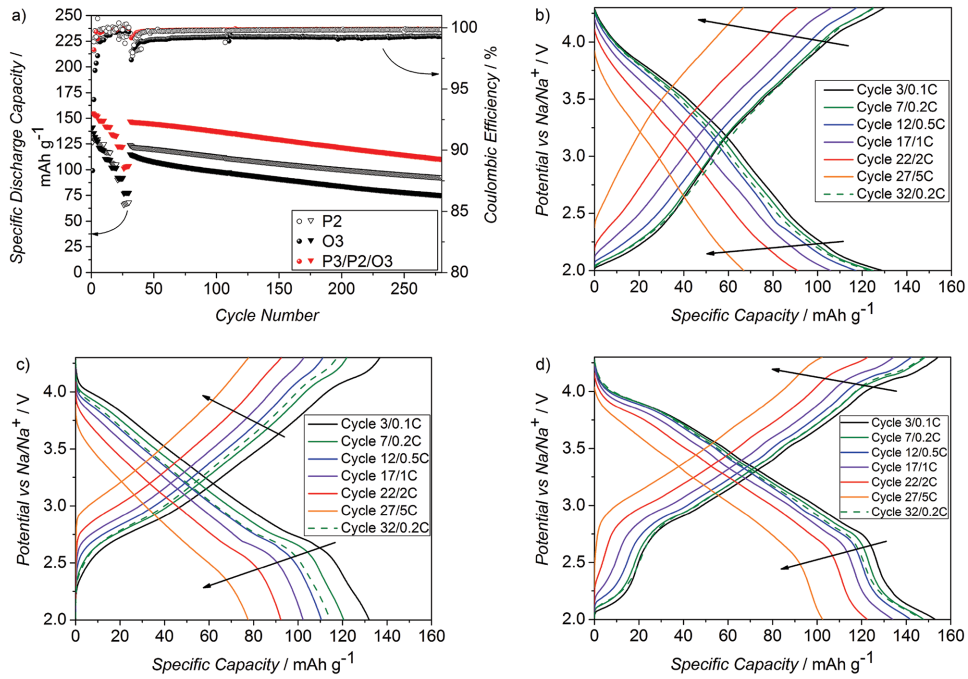

Figure 5. Electrochemical performance of P2-$Na_{2/3}Mn_{0.7}Ni_{0.1}Fe_{0.1}Mg_{0.1}O_2$, O3-$Na_1Mn_{0.5}Ni_{0.3}Fe_{0.1}Mg_{0.1}O_2$, and P3/P2/O3-material during a C-rate test performed at 0.1 C (18 mA g^{-1}), 0.2 C (36 mA g^{-1}), 0.5 C (90 mA g^{-1}), 1 C (180 mA g^{-1}), 2 C (360 mA g^{-1}), 5 C (900 mA g^{-1}) for five cycles each and again 0.2 C (36 mA g^{-1}) for 250 cycles. a) Specific discharge capacities and coulombic efficiencies versus cycle number for 280 cycles, and b–d) potential profiles of selected cycles. Potential range: 2.0–4.3 V versus Na/Na^+. Reference and counter electrode: Na. Temperature: 20 ± 2 °C. Electrolyte: 1 M $NaPF_6$ in PC. Active material mass loading: P2) 4.13 mg, O3) 3.63 mg, P3/P2/O3-material) 4.07 mg.

found in Supporting Information Figure S5. The potential shift and the capacity fading can be interconnected with the Mn^{3+} ion, which can undergo a disproportionation reaction to form Mn^{4+} and Mn^{2+} ions with the latter dissolving into organic electrolytes.[43] This Mn^{2+} dissolution leads to the structural degradation of the material, which is why also a shortening of the potential plateau between 4.0 and 2.5 V can be observed. However, this effect can be prevented by increasing the lower cut-off potential to 2.5 V (which is also more reasonable considering the use of the material in Na-ion cells).

Figure 6a reports the galvanostatic cycling test at 0.1 C (18 mA g^{-1}) of the mixed material in the narrower potential range (2.5–4.3 V). Reduced specific discharge capacities (i.e., 128.2 mAh g^{-1}, 2nd cycle) are obtained as the Mn^{3+}/Mn^{4+} redox process occurring below 2.5 V is avoided. However, the average discharge potential increases from 3.2 to 3.4 V and the capacity fade and structural degradation due to Mn^{2+} dissolution are prevented. As a matter of fact, a more stable cycling behavior and high capacity retention of 85.4% (1st to 200th cycles) can be observed. Furthermore, the coulombic efficiency of the 1st cycle is 95.4%, which is very suitable for full cell applications. The coulombic efficiency is slightly increasing and remains constant at an extraordinary high value of 99.7% throughout cycling. The potential profiles reveal that the cycling is much more stable and the potential plateau are only slightly shifting (Figure 6b). Figure 6c shows a C-rate test for the material using a narrow (2.5–4.3 V) and a wide (2.0–4.3 V) potential range. Increasing the lower cut-off potential leads to an unchanged higher power capability, as nearly the same capacities are obtained at higher rates (5 C) within the two potential ranges. The corresponding discharge potential profiles (Figure 6d) in the narrow potential range (2.5–4.3 V) reveal smaller ohmic drops, i.e., only 0.17 V at higher current rates (5 C, 27th cycle) compared to the wider potential range (Figure 5d). The galvanostatic cycling test of the mixed P3/P2/O3 material at 1 C (180 mA g^{-1}) in the potential range of 2.5–4.3 V demonstrates the excellent material reversibility for 600 cycles (Figure 6e). The average coulombic efficiency exceeds the exceptionally high value of 99.9% throughout the cycling at 1 C. Fingerprint cycles (the 1st and every 50 cycles) were performed at 0.1 C (18 mA g^{-1}) to evaluate material degradations occurring upon cycling. Comparing the specific discharge capacities delivered in these cycles, the extraordinarily high capacity retention of the material is evident (90.2% between the 1st and 601st cycles, both at 0.1 C). Figure 6f shows the potential profiles of the fingerprint cycles, which, by showing only very mild changes, confirm the outstanding reversibility of the (de-)sodiation process in the mixed P3/P2/O3 material. An additional proof comes from the comparison of the electrochemical performance with recently developed state-of-the-art layered sodium oxides reported in Table S5 in

Table 2. Specific discharge capacities obtained for the P2-, O3-, and mixed P3/P2/O3-material at different C-rates (see Figure 5a).

Structure types	0.2 C [mAh g^{-1}]	0.5 C [mAh g^{-1}]	1 C [mAh g^{-1}]	2 C [mAh g^{-1}]	5 C [mAh g^{-1}]
P2	125	117	105	91	67
O3	120	110	102	92	78
P3/P2/O3-material	148	142	134	122	103

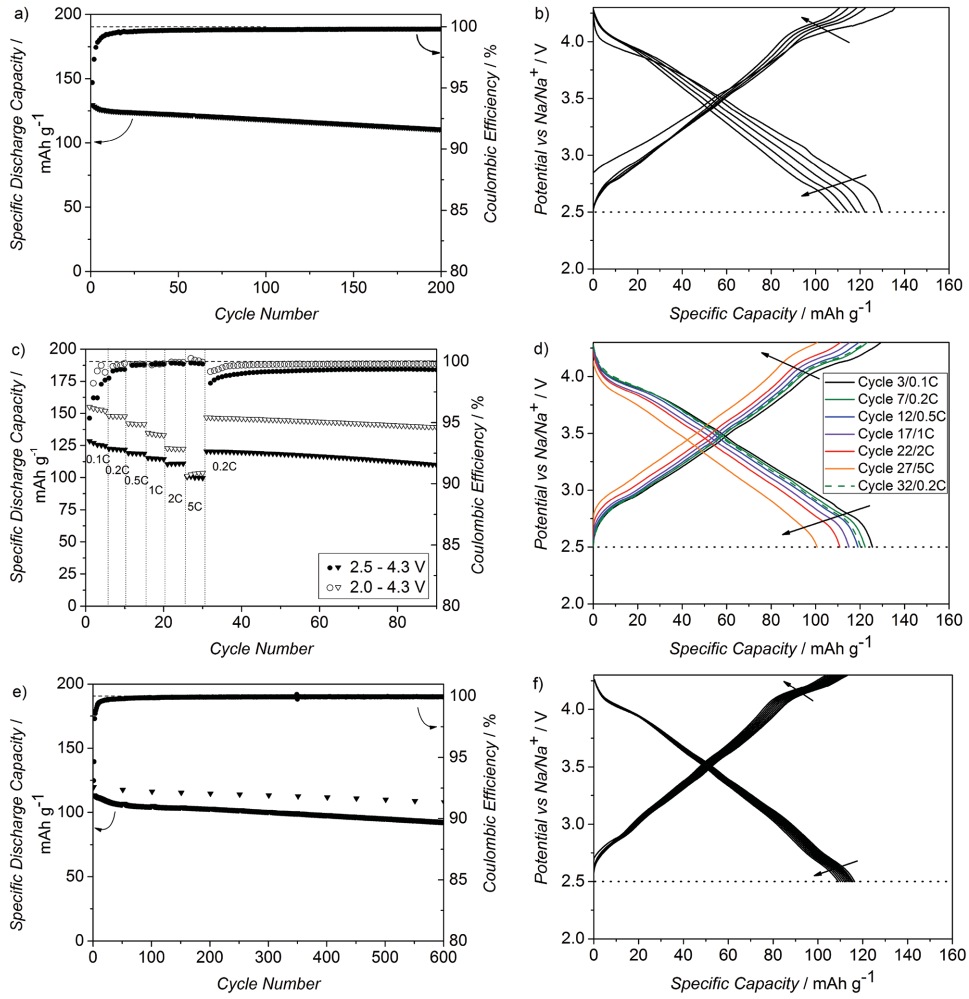

Figure 6. Electrochemical performance of P3/P2/O3-material. a) Galvanostatic cycling test at 0.1 C (18 mA g^{-1}) in a potential range of 2.5–4.3 V. b) Potential profiles at 0.1 C (18 mA g^{-1}) of cycles 1, 50, 100, 150, and 200. c) C-rate test performed at 0.1 C (18 mA g^{-1}), 0.2 C (36 mA g^{-1}), 0.5 C (90 mA g^{-1}), 1 C (180 mA g^{-1}), 2 C (360 mA g^{-1}), 5 C (900 mA g^{-1}), and 0.2 C (36 mA g^{-1}) in different potential ranges. d) Potential profiles of selected cycles. e) Galvanostatic cycling test at 1 C (180 mA g^{-1}), 1st and every 50 cycles at 0.1 C (18 mA g^{-1}) in a potential range of 2.5–4.3 V. f) Potential profiles of fingerprint cycles at 0.1 C (18 mA g^{-1}). Reference and counter electrode: Na. Temperature: 20 ± 2 °C. Electrolyte: 1 M $NaPF_6$ in PC. Active material mass loading: a,b) 3.96 mg, c) 3.98 mg, 4.03 mg, d) 3.98 mg, and e,f) 3.82 mg.

the Supporting Information. This exceptional stable long-term cycling performance of the mixed P3/P2/O3 material in a potential range that is highly suitable for full cell applications, again, proves how promising the unexplored class of mixed P- and O-type structures might be.

3. Conclusion

Novel layered oxide cathode materials containing four different metals (Mn, Ni, Fe, and Mg) were successfully synthesized through a simple and easily upscalable solid state reaction. The feasibility of tuning the structural properties (P2-type or O3-type) of $Na_xMn_yNi_zFe_{0.1}Mg_{0.1}O_2$ by varying the sodium content, the Mn(IV)/Ni(II) ratio and the synthesis conditions, was also demonstrated. With this approach, it was possible to synthesize O3-type $Na_1Mn_{0.5}Ni_{0.3}Fe_{0.1}Mg_{0.1}O_2$ and P2-type $Na_{2/3}Mn_{0.7}Ni_{0.1}Fe_{0.1}Mg_{0.1}O_2$ and, most importantly, the mixed P3/P2/O3-type material with average elemental composition of $Na_{0.76}Mn_{0.5}Ni_{0.3}Fe_{0.1}Mg_{0.1}O_2$. All materials showed good electrochemical performance, but the mixed P3/P2/O3-material revealed outstanding electrochemical performance in terms of specific capacity, rate capability, reversibility, and cycle stability.

This superior performance is the result of different effects. The coexistence of structures in the mixed material has a synergetic effect on the electrochemical performance. The O3-type phase grants a larger initial sodium reservoir (high (initial) specific capacities) and the P2-and P3-type phases enable superior rate capability (facile and fast Na^+ cations migration between face-sharing prismatic sites) and better high-voltage stability. However, it is very important to conduct the synthesis under "equilibrium chemistry" conditions by choosing intermediate synthesis parameters, which allow the simultaneous formation of the different phases. In this way, P-type and O-type phases are formed, all in their most thermodynamically stable elemental composition. This enables improved electrochemical

performance, which cannot be achieved by mixing (postsynthesis) pure P- and O-type phases. Moreover, the P-type and O-type phases might stabilize each other as their *c*-axis parameters exhibit opposing changes upon (de-)sodiation and phase transition. This might reduce the strain inside the electrode and stabilize the cycling behavior of the active material.

The presence of the cubic phase, whose composition seems to be $Mg_{1-x}Ni_xO$ ($x \approx 0.3$), although only accounting for a few percent of the sample mass, might have a beneficial impact on the cycling performance as similar compounds were found to enhance the cycling reversibility of layered oxides. Finally, the combination of the larger flakes (P2) and smaller particles (O3 and P3) results in a more effective utilization of the interstices inside the composite electrode. As a matter of fact, the performance of the P3/P2/O3 material is among the best reported for layered oxides.[34] The potential range of 4.3–2.5 V versus Na/Na^+ certainly allows the formulation of powerful Na-ion cells with suitable anode materials, which is currently under investigation in our labs.[44,45] It should be highlighted that the class of mixed P-/O-type materials is rather unexplored. Thus, potential for further improvements exists. The synthesis conditions could, e.g., be modified to formulate new mixtures with different P-type to O-type ratios. This is especially exciting as the optimal ratio between P-type (higher power) and O-type (higher energy) structures in mixtures is still unknown and could lead to tremendous improvements. In any case, various other parameters deserve to be investigated to explain the synergetic effect resulting in the outstanding electrochemical performance, e.g., the detailed elemental composition of the different P2-, P3-, and O3-type structured layered oxides inside the mixture as well as identify the nature of the still unknown cubic phase via transmission electron microscopy (TEM; chemical composition, crystalline structures, and morphology of particles) and X-ray absorption spectroscopy (XAS; oxidation state of elements and structural information).

4. Experimental Section

Synthesis of $Na_x[M]O_2$ Materials (M = Mn, Ni, Fe, Mg): All chemicals were used as received without further purification. All syntheses were carried out by simple and time-efficient solid-state reaction in air and duplicated, at least, twice to ensure reproducibility. For the solid state reaction stoichiometric portions of sodium carbonate monohydrate (Sigma-Aldrich, ≥99.5%), manganese(II) acetate tetrahydrate (Sigma-Aldrich, ≥99%), nickel(II) acetate tetrahydrate (Sigma-Aldrich, ≥99%), iron(II) acetate (Sigma-Aldrich, ≥99.99%), and magnesium(II) acetate tetrahydrate (Sigma-Aldrich, ≥99%) were mixed according to the desired Na/Mn/Ni/Fe/Mg ratio content (P2-$Na_{2/3}Mn_{0.7}Ni_{0.1}Fe_{0.1}Mg_{0.1}O_2$, O3-$Na_1Mn_{0.5}Ni_{0.3}Fe_{0.1}Mg_{0.1}O_2$, P-/O-$Na_{0.76}Mn_{0.5}Ni_{0.3}Fe_{0.1}Mg_{0.1}O_2$) to yield in 0.02 mole of the final material. After intensive manual grinding, the material was preannealed in an aluminum oxide crucible in an open-air muffle furnace at 500 °C for 6 h (heating rate: 3 °C min^{-1}). After cooling down to room temperature in the furnace, the preannealed material was manually ground and then, as a powder, subjected to high temperature annealing at 800 °C (P2-type material) or 900 °C (O3-type and mixed P3/P2/O3-material) for 6 h (heating rate: 5 °C min^{-1}) in an open-air muffle oven, resulting in the formation of a dark brownish powder that was either quenched in liquid nitrogen (O3-type material) or slowly cooled to ambient temperature inside the oven (P2-type and mixed P3/P2/O3-material). It should be noted that the properties of the furnace as well as the annealing environment (e.g., air flow inside the furnace) have a strong influence on the structure of the final material as well as the ratio of the P-type and O-type structure in the mixed materials. Herein, the heat treatment was conducted in a muffle furnace (model L9/12, Nabertherm).

The products of the different synthesis methods were manually ground after the annealing, screened over a 45 µm sieve and, finally, stored in an argon-filled glovebox. No water treatment of the as-prepared materials was performed at the end of the synthesis to remove the impurities of sodium carbonate formed during the annealing process in air. This is due to the high sensitivity of the O3-type structure, which collapses upon the water rinsing process. Interestingly, the P-type phases were found to remain stable in materials composed of O-type and P-type phases (see Figure S6 and Table S1 in the Supporting Information).

Characterization: X-ray diffractograms were recorded in Bragg-Brentano geometry on Bruker D8 Advance. Si-single crystal sample holders were used and all samples were rotated to reduce anisotropies. All diffractograms were recorded with CuK_α radiation ($\lambda = 0.154$ nm) in the 2Θ range of 10°–90° with a step size of 0.014354° resulting in a 2 h measurement procedure.

Morphological characterization was conducted via SEM with a ZEISS 1550VP Field Emission SEM. For measurements the samples were fixed onto an aluminum sample holder with a conductive carbon tape (Plano G3347).

Elemental composition of the different materials was verified via ICP-OES with an Ultima 2 from Horiba.

Electrode Preparation and Cell Assembly: The electrode slurry was prepared by mixing 85 wt% (0.5 g) of active material with 10 wt% (0.059 g) of conductive agent (SuperC65, TIMCAL; dried under vacuum at 120 °C for 6 d) and 5 wt% of polyvinylidenedifluoride (PVdF; dried at 60 °C for 3 d, Solef 6020, Solvay Polymer specialties) (0.294 g, 10 wt% solution in dried *N*-methyl-2-pyrrolidone (NMP)). NMP was added so that the resulting slurry had a solid content of about 30 wt%. Materials were mixed via ball milling using a ball-to-powder-ratio of about 8 and the slurry was cast on aluminum foil. Following, the electrode film was dried at 120 °C and disk electrodes with a diameter of 12 mm were cut and pressed. The final electrodes were dried at 120 °C under vacuum overnight, weighed, dried again, and then stored in an argon-filled glovebox. The average active material mass loading in the used electrodes ranged between 3.63 and 4.16 mg cm^{-2}. For the direct comparison of the electrochemical performance of different materials always similar mass loadings were used.

Three electrode Swagelok cells were assembled in an argon filled glove box from Mbraun (MB 200B ECO) with oxygen and water content of less than 0.1 ppm. Sodium metal was cut from sodium sticks (Acros Organics, 99.8%), pressed and punched on the current collector, and used as counter and reference electrode. As electrolyte a solution of 1 M $NaPF_6$ (Sigma-Aldrich, ≥99%) in PC (UBE, Japan) was used in combination with a glass fiber separator (Whatman).

Electrochemical Characterization: Cyclic voltammetry was performed on a multichannel potentiostat/galvanostat (VMP3) from Biologic Science Instruments using a scan rate of 1 mV s^{-1} between 2.0 and 4.3 V. Galvanostatic cycling experiments were performed on a Maccor battery cycler (Series 4000) between 2.0 and 4.3 V or 2.5 and 4.3 V. A nominal capacity of 180 mAh g^{-1} (1 C = 180 mA g^{-1}) was used for all materials to ensure direct comparability. All tests were performed in climatic chambers at a temperature of 20 ± 2 °C.

Supporting Information

Supporting Information is available from the Wiley Online Library or from the author.

Acknowledgements

This research received funding from the European Union Seventh Framework Programme (FP7/2007-2013) under grant agreement no.

608621. TIMCAL and SOLVAY are acknowledged for kindly providing Super C65 and PVdF, respectively. Furthermore, M.K. would like to thank L. Wu for SEM measurements and Dr. J. von Zamory for SEM and EDX measurements and L. Chagas and C. Vaalma for fruitful discussions.

Received: August 4, 2015
Revised: October 28, 2015
Published online: November 30, 2015

[1] M. Armand, J.-M. Tarascon, *Nature* **2008**, *451*, 652.
[2] Z. Yang, J. Zhang, M. C. W. Kintner-Meyer, X. Lu, D. Choi, J. P. Lemmon, J. Liu, *Chem. Rev.* **2011**, *111*, 3577.
[3] M. D. Slater, D. Kim, E. Lee, C. S. Johnson, *Adv. Funct. Mater.* **2013**, *23*, 947.
[4] D. L. T. B. Reddy, *D. Linden's T. B. Reddy's Handbook*, 3rd Ed., McGraw-Hill Professional, **2001**, NY, USA.
[5] D. Kundu, E. Talaie, V. Duffort, L. F. Nazar, *Angew. Chem.* **2015**, *127*, 3495; *Angew. Chem. Int. Ed.* **2015**, *54*, 3431.
[6] C. Delmas, C. Fouassier, P. Hagenmuller, *Phys. BC* **1980**, *99*, 81.
[7] J. M. Paulsen, J. R. Dahn, *Solid State Ionics* **1999**, *126*, 3.
[8] N. Yabuuchi, S. Komaba, *Sci. Technol. Adv. Mater.* **2014**, *15*, 043501.
[9] D. Buchholz, L. G. Chagas, M. Winter, S. Passerini, *Electrochim. Acta* **2013**, *110*, 208.
[10] L. G. Chagas, D. Buchholz, C. Vaalma, L. Wu, S. Passerini, *J. Mater. Chem. A* **2014**, *2*, 20263.
[11] I. Hasa, D. Buchholz, S. Passerini, B. Scrosati, J. Hassoun, *Adv. Energy Mater.* **2014**, *4*, 1400083.
[12] I. Hasa, D. Buchholz, S. Passerini, J. Hassoun, *ACS Appl. Mater. Interfaces* **2015**, *7*, 5206.
[13] D. Buchholz, C. Vaalma, L. G. Chagas, S. Passerini, *J. Power Sources* **2015**, *282*, 581.
[14] J. Billaud, G. Singh, A. R. Armstrong, E. Gonzalo, V. Roddatis, M. Armand, T. Rojo, P. G. Bruce, *Energy Environ. Sci.* **2014**, *7*, 1387.
[15] X. Sun, Y. Jin, C.-Y. Zhang, J.-W. Wen, Y. Shao, Y. Zang, C.-H. Chen, *J. Mater. Chem. A* **2014**, *2*, 17268.
[16] X. Wu, J. Guo, D. Wang, G. Zhong, M. J. McDonald, Y. Yang, *J. Power Sources* **2015**, *281*, 18.
[17] S. Komaba, N. Yabuuchi, T. Nakayama, A. Ogata, T. Ishikawa, I. Nakai, *Inorg. Chem.* **2012**, *51*, 6211.
[18] K. Kubota, N. Yabuuchi, H. Yoshida, M. Dahbi, S. Komaba, *MRS Bull.* **2014**, *39*, 416.
[19] J. M. Paulsen, J. R. Dahn, *J. Electrochem. Soc.* **2000**, *147*, 2478.
[20] Y. Lei, X. Li, L. Liu, G. Ceder, *Chem. Mater.* **2014**, *26*, 5288.
[21] B. M. de Boisse, D. Carlier, M. Guignard, C. Delmas, *J. Electrochem. Soc.* **2013**, *160*, A569.
[22] N. Yabuuchi, M. Kajiyama, J. Iwatate, H. Nishikawa, S. Hitomi, R. Okuyama, R. Usui, Y. Yamada, S. Komaba, *Nat. Mater.* **2012**, *11*, 512.
[23] E. Lee, J. Lu, Y. Ren, X. Luo, X. Zhang, J. Wen, D. Miller, A. DeWahl, S. Hackney, B. Key, D. Kim, M. D. Slater, C. S. Johnson, *Adv. Energy Mater.* **2014**, *4*, 1400458.
[24] S. Guo, P. Liu, H. Yu, Y. Zhu, M. Chen, M. Ishida, H. Zhou, *Angew. Chem.* **2015**, *127*, 5992; *Angew. Chem. Int. Ed.* **2015**, *54*, 5894.
[25] V. Palomares, M. Casas-Cabanas, E. Castillo-Martínez, M. H. Han, T. Rojo, *Energy Environ. Sci.* **2013**, *6*, 2312.
[26] F. Fievet, P. Germi, F. de Bergevin, M. Figlarz, *J. Appl. Crystallogr.* **1979**, *12*, 387.
[27] A. M. Salem, M. Mokhtar, G. A. El-Shobaky, *Solid State Ionics* **2004**, *170*, 33.
[28] H.-J. Kweon, S. J. Kim, D. G. Park, *J. Power Sources* **2000**, *88*, 255.
[29] S. J. Shi, J. P. Tu, Y. Y. Tang, X. Y. Liu, Y. Q. Zhang, X. L. Wang, C. D. Gu, *Electrochim. Acta* **2013**, *88*, 671.
[30] C. Li, H. P. Zhang, L. J. Fu, H. Liu, Y. P. Wu, E. Rahm, R. Holze, H. Q. Wu, *Electrochim. Acta* **2006**, *51*, 3872.
[31] V. Duffort, E. Talaie, R. Black, L. F. Nazar, *Chem. Mater.* **2015**, *27*, 2515.
[32] D. Yuan, X. Hu, J. Qian, F. Pei, F. Wu, R. Mao, X. Ai, H. Yang, Y. Cao, *Electrochim. Acta* **2014**, *116*, 300.
[33] J. S. Thorne, R. A. Dunlap, M. N. Obrovac, *J. Electrochem. Soc.* **2013**, *160*, A361.
[34] M. H. Han, E. Gonzalo, G. Singh, T. Rojo, *Energy Environ. Sci.* **2014**, *8*, 81.
[35] X. Wang, M. Tamaru, M. Okubo, A. Yamada, *J. Phys. Chem. C* **2013**, *117*, 15545.
[36] F. R. Beck, Y. Q. Cheng, Z. Bi, M. Feygenson, C. A. Bridges, Z. Moorhead-Rosenberg, A. Manthiram, J. B. Goodenough, M. P. Paranthaman, A. Manivannan, *J. Electrochem. Soc.* **2014**, *161*, A961.
[37] R. Berthelot, D. Carlier, C. Delmas, *Nat. Mater.* **2011**, *10*, 74.
[38] R. Kataoka, T. Mukai, A. Yoshizawa, T. Sakai, *J. Electrochem. Soc.* **2013**, *160*, A933.
[39] Z. Lu, J. R. Dahn, *J. Electrochem. Soc.* **2001**, *148*, A1225.
[40] M. Sathiya, K. Hemalatha, K. Ramesha, J.-M. Tarascon, A. S. Prakash, *Chem. Mater.* **2012**, *24*, 1846.
[41] Z. Lu, J. R. Dahn, *J. Electrochem. Soc.* **2001**, *148*, A710.
[42] D. Buchholz, L. G. Chagas, C. Vaalma, L. Wu, S. Passerini, *J. Mater. Chem. A* **2014**, *2*, 13415.
[43] L. G. Chagas, D. Buchholz, L. Wu, B. Vortmann, S. Passerini, *J. Power Sources* **2014**, *247*, 377.
[44] S. Wenzel, T. Hara, J. Janek, P. Adelhelm, *Energy Environ. Sci.* **2011**, *4*, 3342.
[45] L. Wu, D. Buchholz, D. Bresser, L. Gomes Chagas, S. Passerini, *J. Power Sources* **2014**, *251*, 379.

